JACS
JOURNAL OF THE AMERICAN CHEMICAL SOCIETY

Article

pubs.acs.org/JACS

Tetrahalide Complexes of the $[U(NR)_2]^{2+}$ Ion: Synthesis, Theory, and Chlorine K-Edge X-ray Absorption Spectroscopy

Liam P. Spencer,[†] Ping Yang,[⊥] Stefan G. Minasian,[†,‡] Robert E. Jilek,[†] Enrique R. Batista,*[,†] Kevin S. Boland,[†] James M. Boncella,*[,†] Steven D. Conradson,[†] David L. Clark,[†] Trevor W. Hayton,[§] Stosh A. Kozimor,*[,†] Richard L. Martin,[†] Molly M. MacInnes,[†] Angela C. Olson,[†] Brian L. Scott,[†] David K. Shuh,[‡] and Marianne P. Wilkerson[†]

[†]Los Alamos National Laboratory, Los Alamos, New Mexico 87545, United States
[‡]Lawrence Berkeley National Laboratory, Berkeley, California 94720, United States
[§]University of California, Santa Barbara, California 93106, United States
[⊥]Pacific Northwest National Laboratory, Richland, Washington 99352, United States

Supporting Information

ABSTRACT: Synthetic routes to salts containing uranium bis-imido tetrahalide anions $[U(NR)_2X_4]^{2-}$ (X = Cl^-, Br^-) and non-coordinating NEt_4^+ and PPh_4^+ countercations are reported. In general, these compounds can be prepared from $U(NR)_2I_2(THF)_x$ (x = 2 and R = ^{t}Bu, Ph; x = 3 and R = Me) upon addition of excess halide. In addition to providing stable coordination complexes with Cl^-, the $[U(NMe)_2]^{2+}$ cation also reacts with Br^- to form stable $[NEt_4]_2[U(NMe)_2Br_4]$ complexes. These materials were used as a platform to compare electronic structure and bonding in $[U(NR)_2]^{2+}$ with $[UO_2]^{2+}$. Specifically, Cl K-edge X-ray absorption spectroscopy (XAS) and both ground-state and time-dependent hybrid density functional theory (DFT and TDDFT) were used to probe U−Cl bonding interactions in $[PPh_4]_2[U(N^tBu)_2Cl_4]$ and $[PPh_4]_2[UO_2Cl_4]$. The DFT and XAS results show the total amount of Cl 3p character mixed with the U 5f orbitals was roughly 7−10% per U−Cl bond for both compounds, which shows that moving from oxo to imido has little effect on orbital mixing between the U 5f and equatorial Cl 3p orbitals. The results are presented in the context of recent Cl K-edge XAS and DFT studies on other hexavalent uranium chloride systems with fewer oxo or imido ligands.

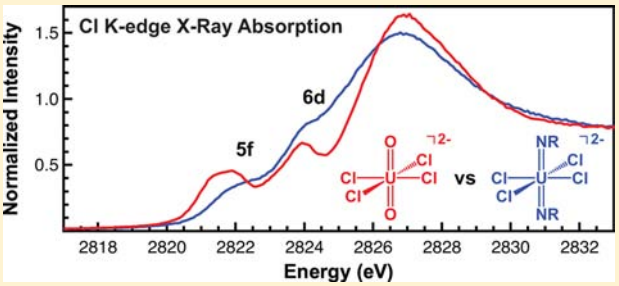

INTRODUCTION

Theoretical and experimental studies on the uranyl ion, $[UO_2]^{2+}$, have provided foundational models for understanding electronic structure and bonding in molecular actinide science.[1−19] Of particular interest are their relevance to understanding the environmental speciation of $[UO_2]^{2+}$, its role in nuclear fuel reprocessing schemes, and its potential as a photocatalyst for solar fuel formation.[20−23] In the course of studying $[UO_2]^{2+}$, the series of dianionic uranyl(VI) tetrahalides—$[UO_2X_4]^{2-}$ (X = Cl, Br, I)—have emerged as popular analytes for spectroscopic and computational studies.[1−19,24−40] These highly symmetric D_{4h} compounds are attractive because they can be prepared in high yields, can be isolated as large single crystals, and are air and moisture stable. Of equal importance, the tetrahalide derivatives can be used as convenient aqueous and nonaqueous starting materials in uranium(VI) synthetic schemes.[41−45]

Despite experimental and theoretical advances that have led to detailed understandings of the U−O interactions in uranyl, little is known about the electronic structure and bonding interactions in other high oxidation state uranium systems. Historically, this has been a direct consequence of the absence of appropriate high-valent analytes for study. Progress in this area may now be achieved with the isolation of U(VI) imido complexes,[46−60] especially those that are isoelectronic with the $[UO_2]^{2+}$ ion. In general, this includes a diverse family of *trans*-oriented bis(imido)uranium(VI) molecules that have similar molecular structures to $[UO_2]^{2+}$. Already many important comparisons have been made between $[U(NR)_2]^{2+}$ and $[UO_2]^{2+}$ ions in terms of reactivity, multiple bond formation with light atoms (i.e., O, N), and the electronic structure of the formal U≡E (E = O, NR) triple bonds. Overall, these studies reveal that—despite many similarities between $[U(NR)_2]^{2+}$ and $[UO_2]^{2+}$—there are significant differences associated with the stability of the axial imido versus oxo functionalities and with the substitution chemistry in the equatorial plane.[46−62]

In our continued studies of the $[U(NR)_2]^{2+}$ ion, we sought to synthesize complexes that could be compared directly with $[UO_2X_4]^{2-}$ in density functional theory (DFT) calculations and

Received: November 1, 2012
Published: January 15, 2013

 © 2013 American Chemical Society

ligand K-edge X-ray absorption spectroscopy (XAS) experiments. To achieve this goal, dianionic bis(imido)uranium(VI) tetrahalide complexes with the general formula $[U(NR)_2X_4]^{2-}$ (R = ^{t}Bu, X = Cl, Br; R = Me, X = Cl; R = Ph, X = Cl) have been synthesized, Table 1. Attempts to isolate the neutral bis(methyl-imido)uranium(VI) derivatives resulted in unexpected formation of the cationic complex $[U(NMe)_2I(THF)_4]^+$, which upon addition of trivalent phosphines or by heating at elevated temperatures under vacuum provided the desired neutral bis(imido)uranium(VI) compounds. In addition to the synthesis of dianionic $[U(N^tBu)_2Cl_4]^{2-}$, we also report theoretical and Cl K-edge XAS[62−70] studies for this compound. The results are compared with the analogous $[PPh_4]_2[UO_2Cl_4]$, and differences in electronic structure between the isoelectronic uranium compounds are discussed. Overall, the results provide experimental evidence that the oxo and imido ligands enhance bonding in the axial positions and limit uranium−ligand orbital mixing in the equatorial plane.

Table 1. Numbering Convention Used for Compounds Investigated in This Study

formula	number
$U(N^tBu)_2I_2(THF)_2$	**1**
$U(NPh)_2I_2(THF)_3$	**2**
$[PPh_4]_2[U(N^tBu)_2Cl_4]$	**3**
$[NEt_4]_2[U(N^tBu)_2Cl_4]$	**4**
$[PPh_4]_2[U(NPh)_2Cl_4]$	**5**
$[NEt_4]_2[U(NPh)_2Cl_4]$	**6**
$[U(NMe)_2I(THF)_4]I_3$	**7**
$U(NMe)_2I_2(THF)_3$	**8**
$U(NMe)_2I_2(DMPE)(THF)$	**9**
$[NEt_4]_2[U(NMe)_2Cl_4]$	**10**
$[NEt_4]_2[U(N^tBu)_2Br_4]$	**11**
$[PPh_4]_2[UO_2Cl_4]$	**12**

EXPERIMENTAL SECTION

Methods and Materials. For synthetic purposes all reactions and manipulations were performed under anaerobic and anhydrous conditions either on a Schlenk line or in a glovebox under an atmosphere of argon. Hexanes and THF were dried by passage over activated alumina, CH_2Cl_2 and CH_3CN (anhydrous) were purchased and stored over activated 4 Å molecular sieves for 24 h before use. CD_2Cl_2 and CD_3CN were dried over activated 4 Å molecular sieves for 24 h before use. $U(N^tBu)_2I_2(THF)_2$ (**1**) and $U(NPh)_2I_2(THF)_3$ (**2**) were synthesized by published procedures.[51,53] Single-crystals of $[PPh_4]_2[UO_2Cl_4]$ (**12**)[71] were obtained from reactions between $[UO_2Cl_2(THF)_2]_2$[72] and two equivalents of PPh_4Cl. The hygroscopic reagents PPh_4Cl and NEt_4X (X = Cl, Br) were dried by dissolving commercially available materials in CH_2Cl_2 followed by addition of a small amount of CaH_2 and allowing the solution to stand overnight. After filtration, the solvent was removed under reduced pressure and the materials were recrystallized from CH_2Cl_2 at −40 °C. All other reagents were purchased from commercial suppliers and used as received. All NMR spectra were recorded on a Bruker AVA300 spectrometer. ^{1}H, ^{13}C{^{1}H}, and ^{31}P{^{1}H} NMR spectra are referenced to external $SiMe_4$ using the residual protio solvent peaks as internal standards (^{1}H NMR experiments), the characteristic resonances of the solvent nuclei (^{13}C NMR experiments), or using H_3PO_4 as an external standard (^{31}P NMR experiments). Elemental analyses were performed at the UC Berkeley Department of Chemistry Microanalytical Facility, on a Perkin-Elmer Series II 2400 CHNS analyzer.

Synthesis of $[M]_2[U(NR)_2Cl_4]$ [R = ^{t}Bu, M = PPh_4 (3), M = NEt_4 (4); R = Ph, M = PPh_4 (5), M = NEt_4 (6)]. The following procedure is representative of the synthesis of complexes **3**−**6**. In the examples with phenyl-imido substituents, reactions were performed in CH_3CN. To a stirred THF (3 mL) solution of $U(N^tBu)_2I_2(THF)_2$ (500 mg, 0.64 mmol) was added a CH_2Cl_2 (3 mL) solution of NEt_4Cl (426 mg, 2.57 mmol). The slurry was stirred overnight and filtered through Celite to yield an orange-red solution. The volume of the solvent was reduced *in vacuo* until several milliliters remained, and then hexanes (10 mL) was added to precipitate a red microcrystalline powder. This powder was isolated by filtration and recrystallized from CH_2Cl_2 (−40 °C) to yield bright red blocks (yield = 84%) that were suitable for single-crystal X-ray diffraction (XRD) experiments. In the case of complex **3**, four molecules of CH_2Cl_2 were present in the solid-state lattice. Under vacuum, the crystalline material obtained readily loses this solvent.

Compound ***3***. ^{1}H NMR (CD_2Cl_2): δ 0.12 (s, 18H, -C(CH_3)$_3$), 7.65 (m, 16H, -PAr*H*), 7.71 (m, 16H, -PAr*H*), 7.75 (m, 8H, -*p*-PAr*H*). ^{13}C{^{1}H} NMR (CD_2Cl_2): δ 30.5 (-C(CH_3)$_3$), 70.7 (-*C*(CH_3)$_3$), 125.6 (-ArC), 131.4 (d, J_{CP} = 13 Hz, -ArC), 135.8 (d, J_{CP} = 10 Hz, -ArC), 136.5 (d, J_{CP} = 3 Hz, -ArC). ^{31}P{^{1}H} NMR (CD_2Cl_2): δ 22.8. Anal. Calcd for $C_{60}H_{66}Cl_{12}N_2P_2U$: C, 46.76; H, 4.32; N, 1.82. Found: C, 46.69; H, 4.30; N, 1.90.

Compound ***4***. Yield = 80%. ^{1}H NMR (CD_2Cl_2): δ 0.16 (s, 18H, -C(CH_3)$_3$), 1.23 (q, *J* = 7 Hz, 24H, -CH_2CH_3), 3.19 (t, *J* = 7 Hz, 16H, -NCH_2). ^{13}C{^{1}H} NMR (CD_2Cl_2): δ 11.5 (-CH_2CH_3), 29.6 (-C(CH_3)$_3$), 32.6 (-NCH_2), 69.3 (-C(CH_3)$_3$). Anal. Calcd for $C_{24}H_{58}Cl_4N_4U$: C, 36.82; H, 7.47; N, 7.16. Found: C, 36.77; H, 7.52; N, 7.22.

Compound ***5***. Yield = 86%. ^{1}H NMR (CD_2Cl_2): δ 5.35 (d, *J* = 8 Hz, 4H, -*o*-Ar*H*), 5.72 (t, *J* = 8 Hz, 2H, -*p*-Ar*H*), 7.01 (d, *J* = 8 Hz, 4H, -*m*-Ar*H*), 7.67 (m, 16H, -PAr*H*), 7.72, (m, 16H, -PAr*H*), 7.75 (m, 8H, -*p*-PAr*H*). ^{13}C{^{1}H} NMR (CD_2Cl_2): δ 118.7 (-ArC_{imido}), 119.6 (-ArC_{imido}), 125.4 (-ArC_{imido}), 125.6 (-ArC), 129.4 (-ArC_{imido}), 131.4 (d, J_{CP} = 13 Hz, -ArC), 135.8 (d, J_{CP} = 10 Hz, -ArC), 136.5 (d, J_{CP} = 3 Hz, -ArC). ^{31}P{^{1}H} NMR (CD_2Cl_2): δ 22.9. Anal. Calcd for $C_{60}H_{50}Cl_4N_2P_2U$: C, 58.07; H, 4.06; N, 2.09. Found: C, 58.13; H, 4.11; N, 2.15.

Compound ***6***. Yield = 75%. ^{1}H NMR (CD_2Cl_2): δ 1.25 (q, *J* = 7 Hz, 24H, -CH_2CH_3), 3.20 (t, *J* = 7 Hz, 16H, -NCH_2), 5.31 (d, *J* = 8 Hz, 4H, -*o*-Ar*H*), 5.68 (t, *J* = 8 Hz, 2H, -*p*-Ar*H*), 7.02 (d, *J* = 8 Hz, 4H, -*m*-Ar*H*). ^{13}C{^{1}H} NMR (CD_2Cl_2): δ 12.9 (-CH_2CH_3), 31.3 (-NCH_2), 117.8 (-ArC_{imido}), 120.2 (-ArC_{imido}), 126.7 (-ArC_{imido}), 130.0 (-ArC_{imido}). Anal. Calcd for $C_{28}H_{50}Cl_4N_4U$: C, 40.87; H, 6.13; N, 6.81. Found: C, 40.92; H, 6.20; N, 6.77.

Synthesis of $[U(NMe)_2I(THF)_4]I_3$ *(****7****).* A mixture of uranium turnings (1 g, 4.20 mmol) and THF (1 mL) was added to a 20 mL scintillation vial and cooled to −25 °C. To this solution were added methylamine (2 M in THF, 13.85 mL, 27.7 mmol, 6.6 equiv) and a THF (3 mL) solution of I_2 (4.8g, 18.9 mmol, 4.5 equiv). After the dark red reaction mixture was stirred overnight, a noticeable white precipitate had formed that was then removed by filtration through Celite. The volatiles were removed *in vacuo*, and the dark red residue was triturated with hexanes (5 mL) followed by addition of diethyl ether (5 mL). The remaining material was suspended in CH_2Cl_2 and washed through Celite until the effluent ran clear and colorless. The volume of the solution was then reduced to approximately 10 mL, layered with an equal amount of diethyl ether, and cooled to −25 °C overnight to yield a dark red microcrystalline material that was rinsed with diethyl ether and dried *in vacuo*. The mother liquor was evaporated to dryness, reconstituted in a minimal amount of CH_2Cl_2, and again layered with diethyl ether to provide a second crop of crystalline material (total 3.62 g, 79% yield) after being cooled to −25 °C for 18 h. ^{1}H NMR (CD_2Cl_2): δ 1.44 (br s, 16H, -CH_2) 3.69 (br s, 16H, -OCH_2), 4.74 (s, 6H, -NCH_3). ^{13}C{^{1}H} NMR (CD_2Cl_2): δ 26.0 (br s, OCH_2CH_2), 58.5 (s, -NCH_3), 73.4 (br s, OCH_2CH_2). Anal. Calcd for $C_{18}H_{38}I_4N_2O_4U$: C, 19.80; H, 3.51; N, 2.56. Found: C, 19.55; H, 3.51; N, 2.56.

Synthesis of $U(NMe)_2I_2(THF)_3$ (8) and $U(NMe)_2I_2$(dmpe)(THF) (9). The following procedure is representative for the synthesis of complexes **8** and **9**. In the synthesis of complex **9**, 2 equiv of dmpe was added to a THF solution of **7**. To a stirring THF solution (3 mL) of $[U(NMe)_2I(THF)_4]I_3$ (200 mg, 0.18 mmol) was added a THF solution (1 mL) of PMe_3 (13.9 mg, 0.18 mmol). The off-red slurry that immediately formed was subsequently stirred for 3 h and then

dx.doi.org/10.1021/ja310575j | J. Am. Chem. Soc. 2013, 135, 2279−2290

filtered through Celite to remove a voluminous white precipitate. The volume of the red filtrate was reduced *in vacuo* until several milliliters remained. Hexanes were added to precipitate a dark red powder, which was recovered by filtration. Recrystallization from CH_2Cl_2/hexanes provides microcrystalline red powder in the case of complex **8** (yield = 91%) and X-ray-quality crystals in the case of complex **9** (yield = 82%).

Compound ***8***. ^{1}H NMR (CD_2Cl_2): δ 2.01 (br s, 12H, -CH_2), 4.32 (br s, 12H, -CH_2), 5.62 (s, 6H, -NCH_3). ^{13}C{^{1}H} NMR (CD_2Cl_2): δ 30.3 (-CH_2), 52.9 (-NCH_3), 72.1 (-OCH_2). Anal. Calcd for $C_{14}H_{30}I_2N_2O_3U$: C, 21.94; H, 3.95; N, 3.66. Found: C, 22.01; H, 4.02; N, 3.68.

Compound ***9***. ^{1}H NMR (CD_2Cl_2): δ 2.16 (br s, 12H, -PCH_3), 2.18 (br s, 4H, -CH_2CH_2), 2.65 (br s, 4H, -PCH_2), 4.49 (br s, 4H, -OCH_2), 5.88 (s, 6H, -NCH_3). ^{13}C{^{1}H} NMR (CD_2Cl_2): δ 18.3 (t, J_{CP} = 7 Hz, -PCH_3), 29.8 (-CH_2), 31.2 (t, J_{CP} = 14 Hz, -PCH_2), 53.8 (-NCH_3), 71.5 (-OCH_2). Anal. Calcd for $C_{12}H_{30}I_2N_2OP_2U$: C, 18.66; %H, 3.92; N, 3.63. Found: C, 18.60; H, 3.95; N, 3.66.

Synthesis of $[NEt_4]_2[U(NMe)_2(Cl)_4]$ (10). To a CH_2Cl_2 (5 mL) solution of NEt_4Cl (303 mg, 1.83 mmol, 4 equiv) in a 20 mL scintillation vial was slowly added a CH_2Cl_2 solution (5 mL) of $[U(NMe)_2I(THF)_4][I_3]$ (500 mg, 0.46 mmol). After being stirred overnight, the dark red slurry was filtered through a plug of Celite, and the precipitate was rinsed with excess CH_2Cl_2. The solid on the Celite was then dissolved and washed through the plug using acetonitrile. This new solution was layered with a small amount of diethyl ether and cooled to −25 °C overnight to yield 171 mg (53%) of a dark red crystalline material. Alternatively, complex **10** could be prepared by addition of 4 equiv of NEt_4Cl to $U(NMe)_2I_2(THF)_3$ in CH_3CN following the same procedure that was described in the synthesis of complexes **3**−**6**. ^{1}H NMR (CD_3CN): δ 1.24 (t, J = 7 Hz, 24H, -CH_3), 3.25 (q, J = 7 Hz, 16H, -NCH_2), 5.61 (s, 6 H, -NCH_3). ^{13}C{^{1}H} NMR (CD_3CN): δ 8.18 (s, -CH_2CH_3), 53.56 (s, -NCH_2CH_3), 57.3 (s, br, -NCH_3). Anal. Calcd for $C_{18}H_{46}Cl_4N_4U$: C, 30.95; H, 6.64; N, 8.02. Found: C, 31.01; H, 6.68; N, 8.09.

Synthesis of $[NEt_4]_2[U(N^tBu)_2Br_4]$ (11). The synthesis of **11** is identical to the procedure described for complexes **5** and **6** (yield = 82%). ^{1}H NMR (CD_2Cl_2): δ 0.38 (s, 18H, -C(CH_3)$_3$), 1.22 (q, J = 7 Hz, 24H, -CH_2CH_3), 3.18 (t, J = 7 Hz, 16H, -NCH_2). ^{13}C{^{1}H} NMR (CD_2Cl_2): δ 12.2 (-CH_2CH_3), 30.0 (-C(CH_3)$_3$), 33.5 (-NCH_2), 70.6 (-C(CH_3)$_3$). Anal. Calcd for $C_{24}H_{58}Br_4N_4U$: C, 30.01; H, 6.09; N, 5.84. Found: C, 30.05; H, 6.16; N, 5.89.

Cl K-Edge X-ray Absorption Spectroscopy Sample Preparation. The XAS samples were prepared in a He-filled glovebox by finely grinding the analyte (7−10 mg) with polystyrene beads (120 mg) for 2 min in a Wig-L-Bug grinder to obtain a homogeneous mixture. An aliquot of this mixture was transferred to a vial, and polystyrene was added, giving a total mass of the final mixture of 90 mg and a chlorine concentration of 6×10^{-5} mmol of Cl/mg total. The new mixture was ground for 2 min in the Wig-L-Bug grinder to achieve small and finely divided particles. An aliquot of this mixture (60 mg) was transferred to a vial, and toluene (c.a. 0.4 mL) was added. The resulting solution was transferred to a 5 mm × 11 mm × 4 mm well in an aluminum sample plate that had been secured to a Teflon block. After 48 h, the toluene had evaporated, and the Teflon plate was removed, leaving a robust film fixed in the sample-plate window.

Cl K-Edge XAS Measurements. The room temperature Cl K-edge XAS data were recorded at the Stanford Synchrotron Radiation Lightsource (SSRL) and analyzed using the 54-pole wiggler beamline 6-2 under ring conditions of 3.0 GeV and 85−100 mA in high magnetic field mode of 0.9 T with a Ni-coated harmonic rejection mirror (detuned to near 50% at 3150 eV) and a Si(111) double crystal monochromator. For these measurements, a chamber similar to that described previously was used,[68−70] with the exception that two additional layers of radiological containment were introduced. The first was a beryllium window (50 μm thick) to separate the I_0 chamber from the beam pipe. The second was a polypropylene window (4.5 μm) used to separate the I_0 and I_1 chambers. Sample fluorescence was measured under vacuum (10^{-7} Torr), and the Cl K-edge XAS data was collected against the incident beam using pairs of backward facing International Radiation Detector XUV100 type photodiodes coated with 1000 Å of Al. The photodiodes were closely spaced so that a 1−2 mm wide beam passed between them. Incident beam intensity was measured from scatter off the He atmosphere with a photodiode pair in a front chamber. Fluorescence from the sample was measured by an identically configured photodiode pair facing the sample that was mounted at normal incidence to the oncoming beam that collected a large solid angle because of its close proximity to the sample (5−10 mm).

The results were reproduced on beamline 4-3 using the 24-pole, 2.0-T wiggler under ring conditions of 300 mA with a bent vertically collimating mirror (1 m, Si, Rh-coated mirror; cutoff ∼4 keV) and a fully tuned Si(111) double crystal monochromator. The data was obtained using the dedicated beamline 4-3 sample chamber under an atmosphere of continually flowing helium. Polystyrene encapsulated uranium samples were isolated from the sample chamber using two polypropylene windows (4 μm). The incident beam intensity was monitored using a helium filled ion chamber and the sample fluorescence was measured using a single element silicon vortex detector, which was positioned sufficiently far from the sample to ensure that dead time was less than 3% over the rising edge.

The energy calibrations for all Cl K-edge XAS spectra were conducted repeatedly between sample scans, and based on the maximum of the first pre-edge feature (2820.20 eV) in the Cl K-edge XAS of D_{2d}-Cs_2CuCl_4,[63−67] which was prepared as described previously.[74] The Cl K-edge XAS data were collected with vertical slit sizes set at 1 mm over three different step sizes, which were 1.00, 0.07, and 1.00 eV for the pre-edge (2705−2801 eV), edge (2801−2835 eV), and post-edge (2835−3140 eV) regions, respectively. To obtain adequate statistics, 1−4 s counting times were employed, and the spectra were collected three times.

XAS Data Analysis. Data manipulation and analysis procedures were similar to those described by Solomon and co-workers.[63−67] For example, in typical data analysis for Cl K-edge XAS, a first-order polynomial was fit to the pre-edge region (2705.0−2810.0 eV) and then subtracted from the experimental data to eliminate the background of the spectrum. The data were normalized by fitting a second-order polynomial to the post-edge region of the spectrum (2860.0−3140.0 eV) and by setting the edge jump at 2836.5 eV to an intensity of 1.0.[63] The normalization procedure gives spectra normalized to a single Cl atom, or M−Cl bond. Curve-fitting analyses were conducted using the mathematical expressions for pseudo-Voigt and step functions employed by EDG_FIT,[75] in an identical manner to that described by Solomon and co-workers.[63] For convenience, we have incorporated these expressions in the program IGOR 6.0. Curve fits were performed over several energy ranges. The first and second derivatives of each spectrum were used as guides to determine the number and position of the spectral features for the curve-fitting analyses. Curve fits utilized pseudo-Voigt line shapes and a step function to model the pre-edge and rising edge spectral features.[63] For the pre-edge and white line features, a fixed 1:1 ratio of Lorentzian to Gaussian contributions were used, and for the step function, a 1:1 ratio of arctangent and error function contributions were employed.[63] The quality of the model was evaluated based on the least-squares correlation coefficients, residual data that only slightly deviated from zero, and symmetric residual peaks.[68−70,76,77] The area under the pre-edge peaks (hereafter defined as the intensity) was compared to the well-established Cl K-edge intensity standard Cs_2CuCl_4. Solomon and co-workers report this feature to have a normalized pre-edge intensity of 0.53 corresponding to 7.5% Cl 3p character.[63] Using our polystyrene encapsulation methodology, we routinely reproduce these pre-edge intensities between 0.50 and 0.55. We take this as evidence that we can reproducibly determine % Cl 3p character to ±5%. Consistently, different samples of crystalline $[PPh_4]_2[UO_2Cl_4]$, **12**, and $[PPh_4]_2[U(N^tBu)_2Cl_4]$, **3**, were examined during three different experimental periods to confirm reproducibility and establish error limits with the measurements. Based on these results, when the pre-edge region of the spectra is modeled with two features, error limits associated with the intensities are estimated at 5%. In contrast, modeling with three features provides appreciably larger error

dx.doi.org/10.1021/ja310575j | J. Am. Chem. Soc. 2013, 135, 2279−2290

associated with the peak width for the two low energy features (<2824 eV), which increases the estimate of intensity error to between 10 and 20%.

Electronic Structure Calculations. Electronic structure calculations were conducted on the $[UO_2Cl_4]^{2-}$ and $[U(N^tBu)_2Cl_4]^{2-}$ dianions using B3LYP hybrid DFT[78,79] in the Gaussian 03 code.[80] The Stuttgart 97 relativistic effective core potential (RECP) and associated basis sets (minus the most diffuse functions with exponents smaller than 0.005) were used for U.[81−83] For the C and H atoms the 6-31G* basis sets were used, while for Cl the 6-31G* basis set was modified by recontracting the p functions to the B3LYP 2p through 6p atomic orbitals of Cl^-.[84] The recontraction of the p space did not change the predicted structures and proved advantageous by providing a cleaner interpretation of the participating atomic orbitals in the molecular orbitals under consideration. These functionals and basis sets have been extensively tested for organometallic systems and shown to give good agreement with experimental data.[85,86] The populations of the Cl 3p orbitals of each compound were then obtained by Mulliken population analysis of each particular molecular orbital.

Time-Dependent Density Functional Theory. For $[UO_2Cl_4]^{2-}$ and $[U(N^tBu)_2Cl_4]^{2-}$, the Cl K-edge XAS spectra were simulated using TDDFT. These calculations were conducted as previously described,[68−70] and involve evaluating core electron excitations by exploiting the small amount of mixing of the core orbitals with the high-lying unoccupied virtual orbitals. Specifically this analysis involves a linear response calculation, for extracting the probability amplitudes from the transition densities and dipole moments between the calculated excited states and the ground states. The excitations originating from all of the intermediate states between the Cl 1s and the HOMO were excluded so that only excitations from the core levels to virtual molecular orbitals could be analyzed. This allows the virtual orbitals to mix and reflect the presence of the core hole in chlorine. Relaxations for the other occupied orbitals associated with the core hole are also not included. Although excluding relaxations in the occupied orbitals associated with the core hole results in large errors associated with absolute calculated transition energies, this computation technique addresses the first order changes in virtual orbitals accompanying the core hole excitation. Previously these calculations have provided very good agreement with experimental measurements made on transition metal compounds.[68−70,76,77] To account for the omission of the atomic relaxation associated with the core excitation, relativistic stabilization, and errors associated with the functional for the closed shell compounds in the calculated spectra were shifted so that the first calculated 6d-peak was equal in energy to the first experimentally determined 6d peak, which involved a shift of 64.31 and 64.14 eV for $[UO_2Cl_4]^{2-}$ and $[U(N^tBu)_2Cl_4]^{2-}$, respectively.

X-ray Crystallographic Details. The crystal structures of compounds **3**, **5**, **7**, **9**, **10**, and **11** were determined as follows, with exceptions noted below: The crystal was mounted in a nylon cryoloop from Paratone-N oil under an argon gas flow. The data were collected on a Bruker SMART APEX II charge-coupled-device diffractometer, with a KRYO-FLEX liquid nitrogen vapor cooling device. The instrument was equipped with a graphite monochromatized Mo Kα X-ray source (λ = 0.71073 Å), with MonoCap X-ray source optics. A hemisphere of data was collected using ω scans, with 5 s frame exposures and 0.3° frame widths. Data collection and initial indexing and cell refinement were handled using APEX II software.[87] Frame integration, including Lorentz-polarization corrections, and final cell parameter calculations were carried out using the SAINT+ software.[88] The data were corrected for absorption using the SADABS program.[89] Decay of reflection intensity was monitored via analysis of redundant frames. Structures were solved using direct methods and difference Fourier techniques. All hydrogen atom positions were idealized and rode on the atom to which they were attached. The final refinement included anisotropic temperature factors on all non-hydrogen atoms. Structure solution, refinement, graphics, and creation of publication materials were performed using SHELXTL.[90] For **5**, the uranium complex was disordered on a 2/*m* symmetry site and atoms in general positions were refined at one-half occupancy. For **9**, the crystal was twinned and the data were indexed, integrated, and refined using a rotation twin law; the batch scale factor refined to 0.3994(6).

RESULTS AND DISCUSSION

Synthesis. The addition of 5 equiv of PPh_4Cl or NEt_4Cl to $U(NR)_2I_2(THF)_X$ [R = ^{t}Bu, X = 2 (**1**); R = Ph, X = 3 (**2**)] in a 1:1 CH_2Cl_2/THF solution generates the dianionic uranium complexes shown in eq 1 with the general formula $[M]_2[U(NR)_2Cl_4]$ [R = ^{t}Bu, M = PPh_4 (**3**), M = NEt_4 (**4**); R = Ph, M = PPh_4 (**5**), M = NEt_4 (**6**)], Table 1. In the case of *tert*-butylimido complexes **3** and **4**, recrystallization from saturated CH_2Cl_2 solutions provided crystalline materials in reasonable yields (>80%), which were characterized by NMR spectroscopy, elemental analysis, and X-ray crystallography. The analogous bis(phenyl-imido)uranium complex **6** was obtained by layering CH_3CN solutions with Et_2O. The ^{1}H NMR spectrum of **3** is representative of all these dianionic complexes and features well-defined aryl resonances at 7.65, 7.71, and 7.75 ppm attributable to the phenyl moieties of the PPh_4^+ cation. Furthermore, there is also a singlet at 0.12 ppm attributable to the *tert*-butyl-imido group. The aryl-imido-substituted complex **5** features similar phenyl resonances at 7.67, 7.72, and 7.75 ppm attributable to the PPh_4^+ cation in addition to resonances at 5.35, 5.72, and 7.01 ppm that arise from the phenyl protons of the imido ligand.

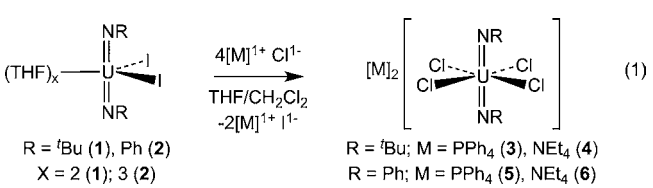

(1)

The solid-state molecular structures of **3** and **5** are representative of these tetrachloride uranium(VI) complexes and are shown in Figure 1. For **3**, there are two independent

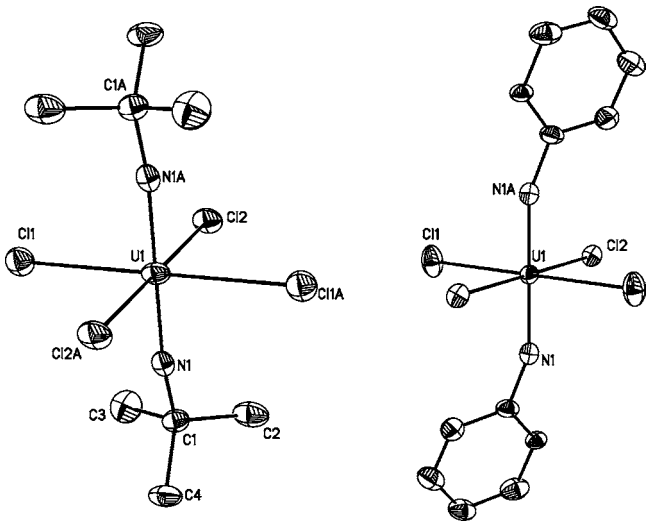

Figure 1. Solid-state molecular structures of $[U(N^tBu)_2Cl_4]^{2-}$ and $[U(NPh)_2Cl_4]^{2-}$ determined for complexes **3** and **5** with thermal ellipsoids drawn at the 50% probability level. Selected bond lengths (Å) and angles (deg): **3**, U1−N1 = 1.816(8), U1−Cl1 = 2.718(3), U1−Cl2 = 2.738(3), N1−U1−N1A = 180.0(5), N1−U1−Cl1 = 88.9(3), N1−U1−Cl2 = 87.0(2); **5**, U1−N1 = 1.842(8), U1−Cl1 = 2.6699(18), U1−Cl2 = 2.682(2), N1−U1−N1A = 180.000(1), N1−U1−Cl1 = 91.4(2), N1−U1−Cl2 = 91.0(2).

dx.doi.org/10.1021/ja310575j | J. Am. Chem. Soc. 2013, 135, 2279−2290

molecules in the unit cell, one of which is shown in Figure 1. Complexes **3** and **5** are six-coordinate with uranium ions bound by *trans*-disposed imido ligands (**3**, N1−U1−N1A = 180.0°; **5**, N1−U1−N1A = 180.0°). The U−N(imido) bond lengths in **3** and **5** (**3**, U1−N1 = 1.816(8) Å; **5**, 1.842(8) Å) are similar to other bis(imido)uranium(VI) complexes as are the average U−Cl bond distances (**3**, U−Cl = 2.728(3) Å; **5**, 2.676(2) Å).[60,98] These U−Cl bond lengths are also similar to the U−Cl bond distances found in the analogous uranyl(VI) dianions $[PPh_4]_2[UO_2Cl_4]$ (2.675(7) Å).[71]

Encouraged by the successful isolation of these ions, we investigated the synthesis of other bis(imido)uranium(VI) dianions, in particular those with methyl-imido ligands. We had anticipated that this would be achieved in a similar synthetic manner to that described above, that is by addition of 4 equiv of NEt_4Cl to the methyl-imido uranium(VI) complex $U(NMe)_2I_2(THF)_3$. Surprisingly, we were unable to synthesize $U(NMe)_2I_2(THF)_3$ by the standard protocols that have been utilized for other *trans*-bis(imido)uranium(VI) complexes. In fact, the reaction between 6 equiv of $MeNH_2$, 3 equiv of I_2, and 1 equiv of uranium turnings does not yield the anticipated neutral uranium(VI) product $U(NMe)_2I_2(THF)_3$. Instead, the cationic species $[U(NMe)_2I(THF)_4]I_3$ (**7**) is recovered in a reasonable yield after recrystallization from THF/hexanes (Scheme 1). Consistent with the product that is recovered

Scheme 1

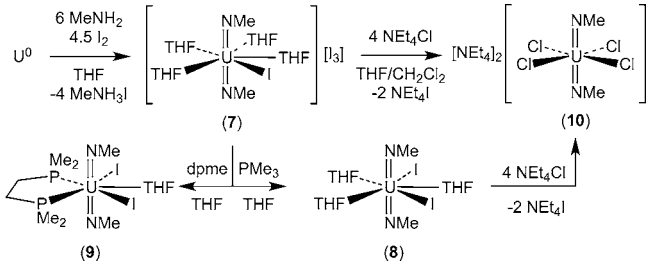

from this reaction, the yield can be significantly increased (79%) by the addition of 4.5 equiv of I_2. The identity of this species was confirmed by X-ray crystallography and the solid-state molecular structure is shown in Figure 2. Complex **7**

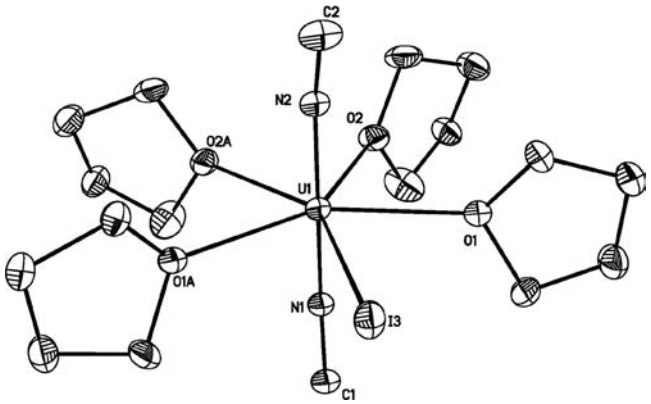

Figure 2. Solid-state molecular structure of $[U(NMe)_2I(THF)_4]^+$ (**7**) with thermal ellipsoids drawn at the 50% probability level. Selected bond lengths (Å) and angles (deg): U1−N1 = 1.830(4), U1−N2 = 1.841(5), U1−I3 = 3.124(5) U1−O1 = 2.474(3), U1−O2 = 2.466(3), N1−U1−N2 = 179.3(2).

features a seven-coordinate uranium center with *trans*-oriented bis(imido) ligands (N1−U1−N1A = 179.3(2)°) and four neutral tetrahydrofuran ligands in the equatorial plane. Furthermore, the average U−N(imido) (1.835(5) Å) and U−I bond distances (3.0864(5) Å) are similar to analogous distances found in other neutral bis(imido)uranium(VI) complexes.[51,52,54,55] The average I−I bond lengths (2.9104(3) Å) found in the triiodide anion are typical of this species.[55b] The ^{1}H NMR spectrum of **6** displays a methyl-imido resonance at 5.44 ppm in addition to broad THF resonances at 1.91 and 4.06 ppm that integrate to four coordinated THF molecules. Additionally, the $^{13}C\{^1H\}$ NMR spectrum features a resonance at 58.5 ppm that can be attributed to the carbon center in the methyl-imido ligand.

With a continued goal to access the $[U(NMe)_2Cl_4]^{2-}$ dianion, we next focused on preparing an appropriate synthetic precursor, namely $U(NMe)_2I_2(THF)_3$ (**8**), via elimination of I_2 from $[U(NMe)_2I(THF)_4]I_3$ (**7**). We discovered that the neutral bis(imido)uranium(VI) species can be isolated by heating solid samples of $[U(NMe)_2I(THF)_4]I_3$ under vacuum at 60 °C for 2 h. Alternatively, the addition of 1 equiv of PMe_3 to **7** in THF provided $U(NMe)_2I_2(THF)_3$ (**8**) in near-quantitative yield (Scheme 1). During the course of this reaction, a voluminous white precipitate formed (likely $[PMe_3I][I]$) that was easily separated by filtration from **8**. The neutral uranium product $U(NMe)_2I_2(THF)_3$ (**8**) was identified by ^{1}H and ^{13}C NMR spectroscopy and elemental analysis. Despite numerous attempts to obtain XRD-quality single crystals, the solid-state molecular structure of this species has yet to be determined. The ^{1}H and ^{13}C NMR spectra show distinctly different resonances than those observed in the cationic species $[U(NMe)_2I(THF)_4]I_3$. For example, the ^{1}H NMR spectrum features a singlet at 5.62 ppm that is assigned to the NMe ligand protons and resonances at 2.01 and 4.32 ppm that can be attributed to the coordinating THF ligands. Integration of these resonances shows that there are only three THF molecules coordinated to the metal center.

To obtain solid-state molecular structure information on the neutral bis(methyl) imido uranium(VI) complex **8**, 1,2-bis(dimethylphosphino)ethane (dmpe) was added to a THF solution of complex **7**. After separating a white precipitate that forms during the course of the reaction, the dmpe-adduct $U(NMe)_2I_2(dmpe)(THF)$ (**9**) was isolated in near-quantitative yield (Scheme 1). This species was characterized by NMR spectroscopy, elemental analysis, and a single-crystal XRD experiment. The room-temperature ^{1}H NMR spectrum of **9** reveals a C_{2v} symmetric species in solution with dmpe resonances at 2.16 and 2.65 ppm in addition to tetrahydrofuran resonances at 2.18 and 4.49 ppm. A singlet attributable to the methyl-imido ligand is observed at 5.88 ppm. Consistent with the C_{2v} symmetric nature of the complex in solution, a singlet at 71.3 ppm is observed in the $^{31}P\{^1H\}$ NMR spectrum.

The solid-state molecular structure of **9** (Figure 3) was determined by a single-crystal XRD experiment on crystals grown by layering hexanes on a THF solution of **9**. Complex **9** possesses a distorted pentagonal bipyramidal geometry at the uranium center with the two methyl-imido ligands assuming axial positions (N1−U1−N1A = 169.2(2)°). The average U−P bond distances (2.920(2) Å) are similar to other bis(imido)-uranium(VI) phosphine complexes $Cp_2U(N^tBu)_2(dmpe)$ (U−P_{ave} = 2.999(10) Å)[55] and $U(N^tBu)_2I_2(PMe_3)_2(THF)$ (U−P_{ave} = 3.059(3) Å).[54] The U−N(imido) and U−I bond distances

dx.doi.org/10.1021/ja310575j | J. Am. Chem. Soc. 2013, 135, 2279−2290

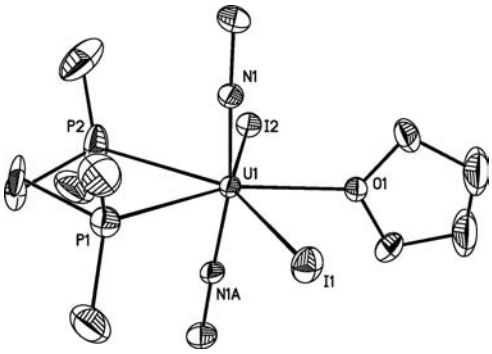

Figure 3. Solid-state molecular structure of $U(NMe)_2I_2(dmpe)(THF)$ (**9**) with thermal ellipsoids drawn at the 50% probability level. Selected bond lengths (Å) and angles (deg): U1−N1 = 1.845(4), U1−O1 = 2.445(4), U1−P1 = 2.9010(18), U1−P2 = 2.930(2), U1−I1 = 3.1572(5), U1−I2 = 3.1238(6), N1−U1−N1A = 169.2(2).

are similar to other previously described *trans*-bis(imido)-uranium(VI) complexes.[51,52,54,55]

The neutral bis(methyl-imido)uranium(VI) compound $U(NMe)_2I_2(THF)_3$ (**8**) displays reactivity toward NEt_4Cl that is similar to $U(NtBu)_2I_2(THF)_3$. For example, the addition of 4 equiv of NEt_4Cl to $U(NMe)_2I_2(THF)_3$ in a 1:1 mixture of THF/CH_2Cl_2 provides the anticipated uranium(VI) dianion $[NEt_4]_2[U(NMe)_2Cl_4]$ (**10**) in 53% yield (Scheme 1). Alternatively, this product can be synthesized by the addition of 4 equiv of NEt_4Cl to the cationic species $[U(NMe)_2I(THF)_4]I_3$ (**7**). The ^1H NMR spectrum of **10** features well-defined resonances at 1.24 and 3.25 ppm attributable to the ethyl moieties of the NEt_4^+ cation. Furthermore, there is a singlet at 5.61 ppm that we assign to the methyl-imido ligand.

X-ray-quality crystals of **10** were grown by layering a CH_3CN solution with Et_2O; the solid-state molecular structure is shown in Figure 4. Complex **10** features a distorted octahedral

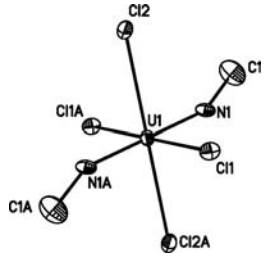

Figure 4. Solid-state molecular structure of $[U(NMe)_2Cl_4]^{2-}$ (**10**) with thermal ellipsoids drawn at the 50% probability level. Selected bond lengths (Å) and angles (deg): U1−N1 = 1.828(6), U1−Cl1 = 2.6941(17), U1−Cl2 = 2.7526(17), N1−U1−N1A = 180.0(5), N1−U1−Cl1 = 91.49(18), N1−U1−Cl2 = 86.11(17).

geometry at the uranium center with *trans*-imido ligands (N1−U1−N1A = 180.0(5)°). The average U−Cl bond distances (2.7099(17) Å) are similar to lengths found in bis(imido)-uranium(VI) tetrachloride complexes **3** and **5** as are the U−N(imido) bond distances.

In light of the successful syntheses of tetrachloride derivatives, we next investigated the syntheses of analogous tetrabromide and tetraiodide bis(imido)uranium(VI) dianions. Using the bis(*tert*-butyl-imido)uranium(VI) platform as a model to determine if such syntheses would be successful, the addition of 4 equiv of NEt_4Br to $U(N^tBu)_2I_2(THF)_2$ in CH_3CN led to the formation of $[NEt_4]_2[U(N^tBu)_2Br_4]$ (**11**) in near-quantitative yield after recrystallization by layering a CH_3CN solution with Et_2O (eq 2). The ^1H NMR spectrum

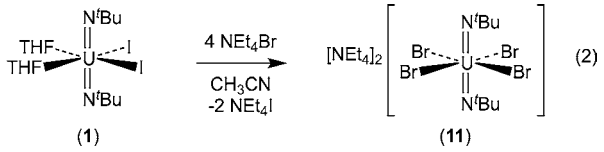

(2)

is consistent with the formation of a tetrabromide derivative as evidenced by a singlet observed at 0.38 ppm for the *tert*-butyl-imido ligand and two multiplets at 1.22 and 3.18 ppm for the ethyl moieties of the NEt_4^+ cation.

The solid-state molecular structure of **11** was determined by X-ray crystallography and is shown in Figure 5. Similar to

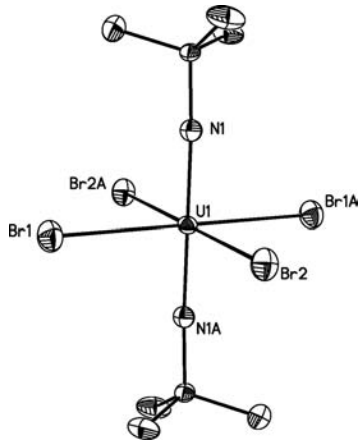

Figure 5. Solid-state molecular structure of $[U(N^tBu)_2Br_4]^{2-}$ (**11**) with thermal ellipsoids drawn at the 50% probability level. Selected bond lengths (Å) and angles (deg): U1−N1 = 1.825(4), U1−Br1 = 2.8513(5), U1−Br2 = 2.8898(5), N1−U1−N1A = 180.0, N1−U1−Br1 = 90.47(12), N1−U1−Br2 = 88.686(16).

tetrachloride analogues, the compound is six-coordinate, and the uranium ion is bound by *trans*-disposed imido ligands (N1−U1−N1A = 180.0°). The average U−Br distances (2.8705(5) Å) are similar to the neutral dibromide complexes $U(N^tBu)_2Br_2(OPPh_3)_2$ (U−Br = 2.8686(16) Å) and $U(N^tBu)_2Br_2(Me_2bpy)$ (Me_2bpy = 4,4′-dimethyl-2,2′-bipyridyl) (U−Br = 2.8297(5) Å)[98] as well as the uranyl complex $[PPh_4]_2[UO_2Br_4]$ ($U-Br_{ave}$ = 2.825(3) Å).[34] Furthermore, the U−N(imido) bond distances are similar to the previously described tetrachloride complexes **3**, **5**, and **9** in addition to other neutral bis(imido)uranium(VI) complexes.[51,52,54,55] Attempts to generate analogous tetraiodide bis(imido)uranium dianionic complexes in reactions between NEt_4I or PPh_4I and $U(N^tBu)_2I_2(THF)_2$ were unsuccessful.

Cl K-Edge XAS. Figure 6 shows the background subtracted and normalized Cl K-edge XAS spectra for polystyrene encapsulated samples of $[PPh_4]_2[UO_2Cl_4]$, **12**, and $[PPh_4]_2[U(N^tBu)_2Cl_4]$, **3**, which are formulated without the non-coordinating countercations hereafter. Both spectra are similar and show multiple pre-edge transitions below 2825 eV with appreciable intensities that are indicative of covalent orbital mixing in the equatorial U−Cl bonds. The pre-edge region of the Cl K-edge spectrum of $[UO_2Cl_4]^{2-}$ is remarkably similar to that of $[U(N^tBu)_2Cl_4]^{2-}$, in that the first and second derivatives indicate that three pre-edge features are present. These features span a wide energy range from about 2819 to 2825 eV and, to a

dx.doi.org/10.1021/ja310575j | J. Am. Chem. Soc. 2013, 135, 2279−2290

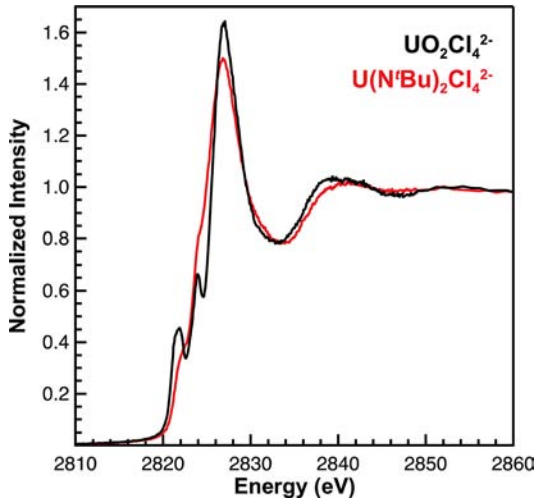

Figure 6. Experimental Cl K-edge X-ray absorption spectra for polystyrene-encapsulated samples of $[PPh_4]_2[UO_2Cl_4]$, **12**, and $[PPh_4]_2[U(N^tBu)_2Cl_4]$, **3**, shown in black and red, respectively.

first approximation, involve excitations of Cl 1s electrons to molecular orbitals that contain primarily U 5f and 6d character.[69,70] The spectra were modeled using symmetrically constrained pseudo-Voigt line shapes with a fixed 1:1 Lorentzian to Gaussian ratio and a step function with a 1:1 ratio of arctangent and error function contributions (Figure 7).

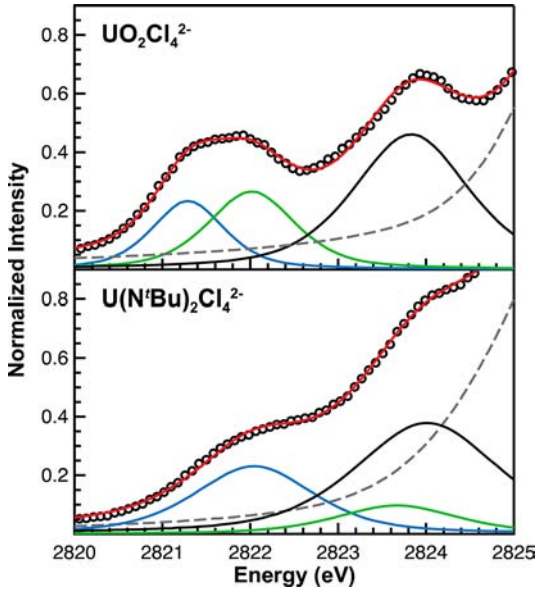

Figure 7. Cl K-edge X-ray absorption spectra for $[PPh_4]_2[UO_2Cl_4]$, **12** (top), and $[PPh_4]_2[U(N^tBu)_2Cl_4]$, **3** (bottom). The data (black ○), curve fits (red trace), pre-edge pseudo-Voigt peaks (blue, green, and black traces), and the post-edge residuals (gray dashed trace), which were generated by subtracting the total fit from the pre-edge pseudo-Voigt peaks, are shown for both species.

A high-quality fit was obtained for both spectra that showed three pre-edge peaks. For $[UO_2Cl_4]^{2-}$ there are two low-energy pre-edge features near 2821 and 2822 eV and a high-energy peak near 2824 eV that is easily resolved from the white line. The spectrum for $[U(N^tBu)_2Cl_4]^{2-}$ is similar in that it contains a low-energy pre-edge feature near 2821 eV, and differs in that two high-energy features are observed near 2824 eV, which are best described as shoulders on the rising edge.

Ground-State Electronic Structure Calculations. Ground-state DFT calculations were conducted on $[UO_2Cl_4]^{2-}$ and $[U(N^tBu)_2Cl_4]^{2-}$ to form a basis for our interpretations of the Cl K-edge XAS shown in Figures 6 and 7. Because the occupied molecular orbitals in $[UO_2Cl_4]^{2-}$ and $[U(N^tBu)_2Cl_4]^{2-}$ have been discussed in detail previously,[1−19,51−54] this discussion will focus on the unoccupied antibonding orbitals that are most relevant to the Cl K-edge XAS experiment. As expected, our DFT calculations for $[UO_2Cl_4]^{2-}$ show strong mixing in a D_{4h} ligand field with the axial oxo ligands. Consistent with previous reports, the U−O interaction is characterized by six antibonding orbitals of $2e_u$ ($5f_\pi$), $1a_{2u}$ ($5f_\sigma$), $1a_{1g}$ ($6d_\sigma$), and $1e_g$ ($6d_\pi$) symmetry, Figure 8.[1−19,24−41] In comparison to the highly covalent U−O bonds, the equatorial Cl ligands are calculated to form U−Cl interactions that have far less Cl 3p-character. The Cl 3p σ-type symmetry-adapted linear combinations (SALCs) of atomic orbitals span $e_u + a_{1g} + b_{1g}$ symmetries and can mix with U 5f and 6d orbitals to form U−Cl σ-bonding interactions of $2e_u$ (U−Cl $5f_\sigma$, U−O $5f_\pi$), $1a_{1g}$ (U−Cl $6d_\sigma$, U−O $6d_\sigma$), and $1b_{1g}$ (U−Cl $6d_\sigma$, U−O $6d_\delta$) symmetries (Figure 8 and Table 2). In contrast, the chlorine π-SALCs of $b_{2u} + b_{2g} + a_{2u} + e_g$ symmetries can mix with U 5f and 6d orbitals to form U−Cl π-bonding interactions of $1b_{2u}$ (U−Cl $5f_\pi$, U−O $5f_\delta$), $1b_{2g}$ (U−Cl $6d_\pi$, U−O $6d_\delta$), $1a_{2u}$ (U−Cl $5f_\pi$, U−O $5f_\sigma$) and $1e_g$ (U−Cl $6d_\pi$, U−O $6d_\pi$) symmetries. Finally, the Cl 3p and U 5f orbitals of $1e_u$ symmetry can mix to form both $\sigma + \pi$ U−Cl bonding interactions (U−Cl $5f_{\sigma+\pi}$, U−O $5f_\varphi$). This leaves the U 5f orbital of $1b_{1u}$ (U−Cl $5f_\delta$, U−O $5f_\delta$; LUMO) symmetry as nonbonding with respect to both O and Cl and the chlorine π-SALC of a_{2g} symmetry (HOMO) as a nonbonding set of chlorine lone pairs.

In the experimental Cl K-edge XAS of the closed-shell D_{4h}-$[UO_2Cl_4]^{2-}$ anion, only transitions from the $^1A_{1g}$ ground state to spin- and electric-dipole-allowed $^1A_{2u}$ and ^1E_u excited states will be observed. Based on the quantitative molecular orbital energies provided from the ground-state DFT calculation (Figure 9), the first pre-edge feature in the Cl K-edge XAS of $[UO_2Cl_4]^{2-}$ is reasonably assigned to closely spaced excitations from the Cl 1s orbitals to empty molecular orbitals of $1b_{2u}$ ($^1A_{1g} \rightarrow {}^1A_{2u}$) and $1e_u$ ($^1A_{1g} \rightarrow {}^1E_u$) symmetry. The two higher energy features are assigned to transitions involving the second, higher-energy set of $2e_u$ ($^1A_{1g} \rightarrow {}^1E_u$) and $1b_{2g}$ orbitals ($^1A_{1g} \rightarrow {}^1E_u$), respectively.

The general composition and relative energies of the valence molecular orbitals in $[U(N^tBu)_2Cl_4]^{2-}$ are quite similar to those for $[UO_2Cl_4]^{2-}$.[51−54] For example, ignoring the *tert*-butyl substituents on the imido ligand and assuming D_{4h} symmetry for $[U(N^tBu)_2Cl_4]^{2-}$, the imido functionality in $[U(N^tBu)_2Cl_4]^{2-}$ can be regarded as a formal U≡N^{t}Bu triple bond that is composed of both U−N σ and π bonding interactions involving the uranium orbitals of $2e_u$ (U−N $5f_\pi$, U−Cl $5f_\sigma$), $1a_{2u}$ (U−N $5f_\sigma$, U−Cl $5f_\pi$), $1a_{1g}$ (U−N $6d_\sigma$, U−Cl $6d_\sigma$), and $1e_g$ (U−N $6d_\pi$, U−Cl $6d_\pi$) symmetry. In addition, the unoccupied orbitals of $1b_{1u}$ (U−Cl $5f_\delta$, U−N $5f_\delta$), $1b_{2u}$ (U−Cl $5f_\pi$, U−N $5f_\delta$), $1e_u$ (U−Cl $5f_{\sigma+\pi}$, U−N $5f_\varphi$), and $1b_{2g}$ (U−Cl $6d_\pi$, U−N $6d_\delta$) symmetries are similar in energy to that observed for $[UO_2Cl_4]^{2-}$, Figure 9 and Table 2. Hence, the Cl K-edge XAS spectrum of $[U(N^tBu)_2Cl_4]^{2-}$ can be interpreted in analogy to $[UO_2Cl_4]^{2-}$ as involving Cl 1s electron excitations to the low lying $1b_{2u}$, $1e_u$, $2e_u$, and $1b_{2g}$, orbitals. However for

dx.doi.org/10.1021/ja310575j | J. Am. Chem. Soc. 2013, 135, 2279−2290

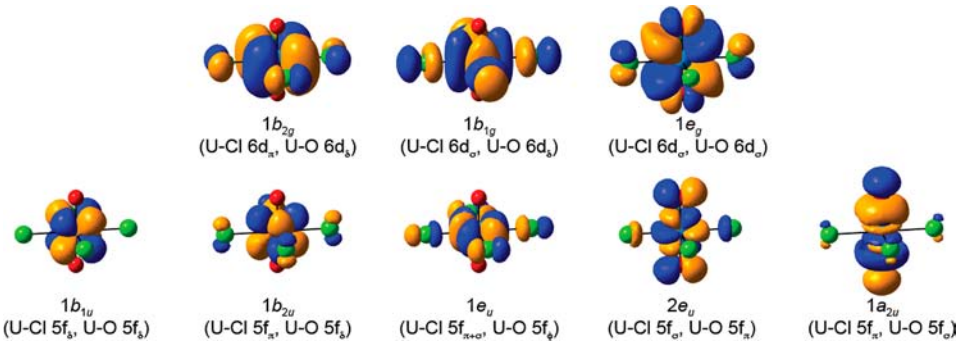

Figure 8. Representative virtual Kohn–Sham orbitals for D_{4h}-$UO_2Cl_4^{2-}$ showing the U–Cl and U–O antibonding interactions, with the exception that the virtual $1a_{1g}$ (U–Cl $6d_\sigma$, U–O $6d_\sigma$) is not included because it is so high in energy.

Table 2. Comparison of the Experimental and Calculated Pre-Edge Peak Energies (eV) and Amounts of Cl 3p Character (%)[a] for the Polystyrene-Encapsulated Compounds $[PPh_4]_2[UO_2Cl_4]$, 12, and $[PPh_4]_2[U(N^tBu)_2Cl_4]$, 3

		energy (eV)		Cl 3p character (%)[a]	
assignment	final state orbital	exptl	calcd	exptl	calcd
		D_{2d}-$CuCl_4^{2-}$			
1s → 3d	b_{1g}	2820.21[c]	–	7.5[c]	–
		$[PPh_4]_2[UO_2Cl_4]$			
1s → 5f[b]	$1e_u$	2821.29	2820.88	7.6(7)	8.0
	$1b_{2u}$		2820.91		
	$2e_u$	2822.01	2822.64		
1s → 6d	$1b_{2g}$	2823.83	2823.83	10.2(5)	4.2
		$[PPh_4]_2[U(N^tBu)_2Cl_4]$			
1s → 5f	$1e_u$	2822.04	2821.20	7.5(7)	9.7
	$1b_{2u}$		2821.37		
	$2e_u$	2823.67	2822.71		
	$1a_{2u}$		2823.04		
1s → 6d	$1b_{2g}$	2424.01	2824.01	10.4(5)	10.0

[a]The calculated amounts of Cl 3p character (%) per bond were determined by multiplying the total Cl 3p character (determined from the ground-state Mulliken populations) by the sum of the squares of the normalization constants for the corresponding ligand-orbital wave functions (see Table 3).[70,91] [b]Transitions to the 5f orbital of a_{2u} symmetry were not experimentally resolved for $[UO_2Cl_4]^{2-}$ and are not included in the tabulated values for the experimental or calculated amounts of Cl 3p character. Calculations indicate that the amount of Cl 3p character in the orbital of a_{2u} symmetry is small for $[UO_2Cl_4]^{2-}$ (1.0% per U–Cl bond). [c]Reference 63. Error bars are estimated at 5%.

the $[U(N^tBu)_2Cl_4]^{2-}$ dianion, the $1a_{2u}$ orbital (U–Cl $5f_\pi$, U–N $5f_\sigma$) is appreciably lower in energy than observed for $[UO_2Cl_4]^{2-}$. Based on these calculations, we anticipate that the Cl 1s → $1a_{2u}$ ($^1A_{1g} \rightarrow {}^1A_{2u}$) transitions for $[U(N^tBu)_2Cl_4]^{2-}$ are lower in energy than transitions to the $1b_{2g}$ orbital (U–Cl $6d_\pi$, U–N $6d_\delta$) and similar in energy to transitions involving the higher-lying 5f orbitals of $2e_u$ symmetry. Hence, these DFT calculations suggest that all transitions involving U 5f orbitals for $[U(N^tBu)_2Cl_4]^{2-}$ can be experimentally resolved from the rising edge.[93]

Hybrid DFT Spectral Simulations. To better understand the origin of the pre-edge features in the Cl K-edge XAS spectra

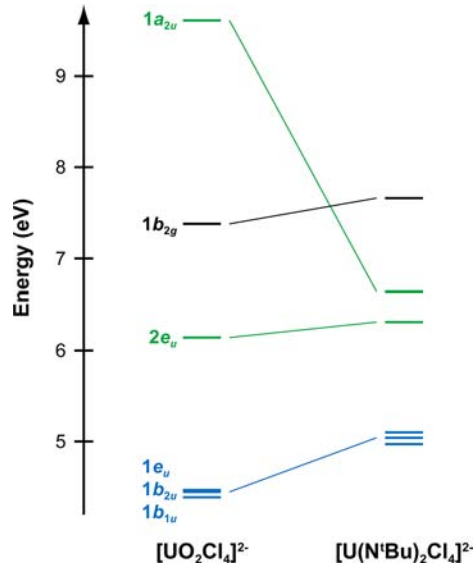

Figure 9. Quantitative correlation diagram showing the 5f orbital contributions to bonding for $[UO_2Cl_4]^{2-}$ and $[U(N^tBu)_2Cl_4]^{2-}$.[92] Molecular orbital energies for both molecules have been shifted by a constant so that the energies of the Cl 1s orbitals are equivalent.

for $[UO_2Cl_4]^{2-}$ and $[U(N^tBu)_2Cl_4]^{2-}$, TDDFT calculations were used to calculate the relative energies and oscillator strengths for the pre-edge transitions, as shown in Figure 10. In the past, TDDFT has helped guide interpretations of ligand K-edge XAS data for a number of closed shell transition metal, uranium, and thorium systems.[69,70] The TDDFT simulated spectra for $[UO_2Cl_4]^{2-}$ and $[U(N^tBu)_2Cl_4]^{2-}$ were shifted by +64.31 and +64.14 eV, respectively, such that the energies of the first calculated and experimental transitions to molecular orbitals of $1b_{2g}$ symmetry are equal. This operation accounts for the omission of atomic and extra-atomic relaxation associated with the core excitation, relativistic stabilization, and various errors associated with the functional (see Experimental Section).[94,85]

The TDDFT calculations for $[UO_2Cl_4]^{2-}$ and $[U(N^tBu)_2Cl_4]^{2-}$ are consistent with the group theory analysis, and show four low energy transitions that involve orbitals of $1b_{2u}$, $1e_u$, $2e_u$, and $1b_{2g}$ symmetries (Table 2 and Figure 10). For $[UO_2Cl_4]^{2-}$, transitions involving the $1e_u$ ($^1A_{1g} \rightarrow {}^1E_u$) and $1b_{2u}$ ($^1A_{1g} \rightarrow {}^1A_{2u}$) orbitals are calculated to be lowest with nearly degenerate energies of 2820.88 and 2820.91 eV, respectively. These values compare well with the energy of the first pseudo-Voigt function used in the curve fit, which was observed at

dx.doi.org/10.1021/ja310575j | J. Am. Chem. Soc. 2013, 135, 2279–2290

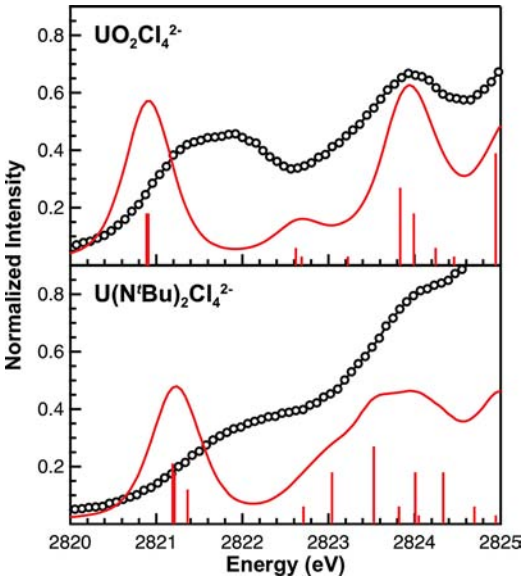

Figure 10. Cl K-edge X-ray absorption spectra (black ○), TDDFT-calculated spectra (red lines), and calculated transitions (red bars) for $[PPh_4]_2[UO_2Cl_4]$, **12** (top), and $[PPh_4]_2[U(N^tBu)_2Cl_4]$, **3** (bottom). The absolute energy for the TDDFT calculated transitions and simulated spectra are adjusted based on experimental data, and the height of the calculated transitions gives the relative oscillator strengths (see Experimental Section).

2821.29 eV (Table 2). Transitions involving the $2e_u$ ($^1A_{1g} \rightarrow {}^1E_u$) and $1b_{2g}$ ($^1A_{1g} \rightarrow {}^1E_u$) orbitals are calculated to be 1.75 and 2.94 eV higher in energy, respectively, which is consistent with energies of the second and third pseudo-Voigt functions used in the curve fit. The TDDFT calculation for $[U(N^tBu)_2Cl_4]^{2-}$ is similar to $[UO_2Cl_4]^{2-}$ in that it also shows a low-energy pre-edge feature arising from two nearly degenerate transitions involving the $1e_u$ and $1b_{2u}$ orbitals, which have energies of 2821.20 and 2821.37 eV, respectively. The TDDFT for $[U(N^tBu)_2Cl_4]^{2-}$ differs in that it shows two transitions at higher energy that involve the remaining U 5f orbitals, one associated with the $2e_u$ orbitals at 2822.71 eV and another only slightly higher in energy that involves the $1a_{2u}$ orbital at 2823.04 eV. These calculated transitions energies agree well with the energy of the second feature used in the experimental curve fit (2823.67 eV).

Evaluation of M−Cl Orbital Mixing. The amount of Cl 3p character (%) in the antibonding molecular orbitals for $[UO_2Cl_4]^{2-}$ and $[U(N^tBu)_2Cl_4]^{2-}$ was determined from the intensities of pre-edge features in the Cl K-edge XAS using the well-established intensity standard, D_{2d}-Cs_2CuCl_4, Table 2.[63−67] Experimentally evaluating the amount of Cl 3p character (%) associated with the individual U 5f pre-edge features is difficult because they are close in energy. Hence, deconvoluting the low-energy U 5f pre-edge peaks with multiple curve-fitting functions resulted in substantially large peak intensity error (estimated at 10−20% at one standard deviation). With these considerations in mind, the lowest energy transitions to the $1e_u$ and $1b_{2u}$ antibonding orbitals in the XAS of $[UO_2Cl_4]^{2-}$ were associated with a pre-edge feature with an intensity of 0.23, which corresponds to 3.2% Cl 3p character per U−Cl bond for both orbitals combined. This value is in reasonable agreement with the sum (4.7%) of individual $1e_u$ (3.8%) and $1b_{2u}$ (0.9%) orbital compositions obtained from the Mulliken population analysis, which are 3.8% and 0.9% Cl 3p character per bond, respectively (as shown in Table 2). Values for $[U(N^tBu)_2Cl_4]^{2-}$ show a similar amount of Cl 3p character with the U 5f orbitals of $1e_u$ and $1b_{2u}$ symmetry whether evaluated using XAS or with DFT (5.3% and 4.9%, respectively). The second pre-edge features in the XAS of $[UO_2Cl_4]^{2-}$ and $[U(N^tBu)_2Cl_4]^{2-}$ have intensities that correspond to 4.4% ($2e_u$) and 2.2% ($2e_u + 1a_{2u}$) Cl 3p character per U−Cl bond, respectively. For comparison, DFT finds the amount of Cl 3p character in the $1a_{2u}$ symmetric orbital for $[UO_2Cl_4]^{2-}$ to be 1.0% per U−Cl bond, however; this metric was not experimentally evaluated because of the high energies of the transition.

The totaled amount of Cl 3p character (%) in the U 5f orbitals can be evaluated with confidence experimentally by fitting the pre-edge region of the spectrum with only two features (Table 2; see XAS Data Analysis section in the Experimental Section). For example, for $[U(N^tBu)_2Cl_4]^{2-}$, the experimental values show a total of 7.5(7)% Cl 3p character per U−Cl bond in the orbitals of $1e_u$, $1b_{2u}$, $2e_u$, and $1a_{2u}$ combined, which compares well with the calculated value of 9.7%, Table 2.

Table 3. Metal s, p, d, and f Orbitals and Symmetry-Adapted Ligand Orbitals for a D_{4h} Complex[a]

		axial ligand orbitals		equatorial ligand orbitals	
representation	metal orbital	σ	π	σ	π
a_{1g}	s, d_{z^2}	$(1/\sqrt{2})(\sigma_5 + \sigma_6)$		$(1/2)(\sigma_1 + \sigma_2 + \sigma_3 + \sigma_4)$	
a_{2g}					$(1/2)(x_1 - y_2 + y_3 - x_4)$
b_{1g}	$d_{x^2-y^2}$			$(1/2)(\sigma_1 - \sigma_2 + \sigma_3 - \sigma_4)$	
b_{2g}	d_{xy}				$(1/2)(x_1 + y_2 + y_3 + x_4)$
e_g	d_{xz}		$(1/\sqrt{2})(y_5 + x_6)$		$(1/\sqrt{2})(y_1 + x_3)$
	d_{yz}		$(1/\sqrt{2})(x_5 + y_6)$		$(1/\sqrt{2})(x_2 + y_4)$
a_{2u}	p_z, f_{z^3}	$(1/\sqrt{2})(\sigma_5 + \sigma_6)$			$(1/2)(y_1 + x_2 - x_3 - y_4)$
b_{1u}	f_{xyz}				
b_{2u}	$f_{z(x^2-y^2)}$				$(1/2)(y_1 - x_2 - x_3 + y_4)$
e_u	p_x		$(1/\sqrt{2})(x_5 - y_6)$	$(1/\sqrt{2})(\sigma_1 - \sigma_3)$	$(1/\sqrt{2})(y_2 - x_4)$
	p_y		$(1/\sqrt{2})(y_5 - x_6)$	$(1/\sqrt{2})(\sigma_2 - \sigma_4)$	$(1/\sqrt{2})(x_1 - y_3)$
	f_{xz^2}		$(1/\sqrt{2})(x_5 - y_6)$	$(1/\sqrt{2})(\sigma_1 - \sigma_3)$	
	f_{yz^2}		$(1/\sqrt{2})(y_5 - x_6)$	$(1/\sqrt{2})(\sigma_2 - \sigma_4)$	
	$f_{x(x^2-3y^2)}$			$(1/\sqrt{2})(\sigma_1 - \sigma_3)$	$(1/\sqrt{2})(y_2 - x_4)$
	$f_{y(3x^2-y^2)}$			$(1/\sqrt{2})(\sigma_2 - \sigma_4)$	$(1/\sqrt{2})(x_1 - y_3)$

[a]The D_{4h} coordinate system was adapted from the one used for an octahedral complex by Ballhausen and Gray.[91]

dx.doi.org/10.1021/ja310575j | J. Am. Chem. Soc. 2013, 135, 2279−2290

Transitions to the $1a_{2u}$ orbital were not resolved for $[UO_2Cl_4]^{2-}$, however, the total Cl 3p character in the $1e_u$, $1b_{2u}$, and $2e_u$ orbitals was determined at 7.6(7)% (XAS) and 8.0% (DFT) per U−Cl bond. Taken together, all the data indicate that the total amount of Cl 3p character in the equatorial U−Cl bonding interactions involving 5f orbitals is approximately 7−10% for both $[UO_2Cl_4]^{2-}$ and $[U(N^tBu)_2Cl_4]^{2-}$. For the U 6d orbitals of $1b_{2g}$ symmetry, statistically identical values of Cl 3p character (%) were determined experimentally for $[UO_2Cl_4]^{2-}$ and $[U(N^tBu)_2Cl_4]^{2-}$ at 10.2(5)% and 10.4(5)%, respectively (Table 2). The experimental value for $[U(N^tBu)_2Cl_4]^{2-}$ is in good agreement with the calculation (10.0%); however, for $[UO_2Cl_4]^{2-}$ somewhat less Cl 3p character was calculated in the $1b_{2g}$ orbital (4.2%).

In an earlier publication,[70] the amount of Cl 3p character per U−Cl bond was evaluated for uranium hexavalent chlorides, namely UCl_6 (DFT, 45.9%) and $[UOCl_5]^-$ (XAS, 26(1)%; DFT, 47.3%). The effect of substituting chloride for oxo and imido ligands can now be examined by comparing the calculated % Cl 3p character for four of the Cl ligands in hexavalent UCl_6, $[UOCl_5]^-$, $[UO_2Cl_4]^{2-}$, and $[U(N^tBu)_2Cl_4]^{2-}$ (Scheme 2). However, to make appropriate comparisons

Scheme 2

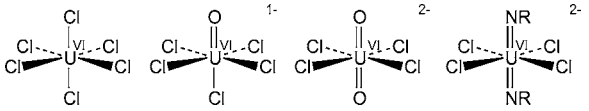

between the amount of Cl 3p character per equatorial U−Cl bond in $[UOCl_5]^-$, $[UO_2Cl_4]^{2-}$, and $[U(N^tBu)_2Cl_4]^{2-}$ with UCl_6, the hexavalent hexachloride calculated values need to be adjusted to four Cl ligands. To achieve this, the total amount of Cl 3p character in the primarily U 5f antibonding orbitals of UCl_6 (DFT, 45.9%) was multiplied by $^4/_6$ to give 30.6% Cl 3p character for four Cl atoms. For the hexavalent mono-oxo species $[UOCl_5]^-$, DFT calculates 23.3% Cl 3p character in each equatorial U−Cl bond. Hence, mixing decreases by approximately $^1/_4$ on substituting one Cl in UCl_6 for one oxo to generate $[UOCl_5]^-$ (30.6% to 23.3%). Substitution of an additional Cl in $[UOCl_5]^-$ for an oxo ligand to generate $[UO_2Cl_4]^{2-}$ decreases the Cl 3p character by an additional $^2/_3$ (23.3% to 8.0%), as does substituting one oxo and one Cl for two imidos to make $[U(N^tBu)_2Cl_4]^{2-}$ (23.3% to 9.7%). Because transitions associated with the higher-lying orbitals of 6d symmetry were not resolved in the Cl K-edge XAS, additional experimentation is needed to place this observation in appropriate context. However, this study points to a significantly reduced role for the U 5f orbitals in interacting with the equatorial Cl ligands in $[UO_2Cl_4]^{2-}$ and $[U(N^tBu)_2Cl_4]^{2-}$ relative to other hexavalent species with fewer oxo or imido ligands.

CONCLUDING REMARKS

The results described above include syntheses for a family of uranium bis-imido tetrahalide complexes of general formula $[U(NR)_2X_4]^{2-}$ (R = alkyl or aryl; X = halide), which are well-suited to systematic theoretical and spectroscopic investigations of electronic structure and bonding in hexavalent uranium compounds. The synthetic approach is best described as ionic salt metathesis, and in general involves addition of multiple equivalents of halide to neutral $U(NR)_2I_2(THF)_x$ precursors. This procedure is versatile, and enables isolation of $[U(NR)_2Cl_4]^{2-}$ compounds in large quantities and in high purity for R = Me, ^{t}Bu, and Ph. The synthetic approach is not limited to cases where the equatorial ligand is chloride, and for methylimido uranium complexes the analogous bromide compound was also prepared.

The Cl K-edge XAS results demonstrate a major role for axial oxo and imido ligands in restricting mixing between U 5f orbitals and ligand orbitals in the equatorial plane. Pre-edge features associated with transitions to the U 5f orbitals of $1e_u$, $1b_{2u}$, and $2e_u$ symmetry were identified in the spectra of $[PPh_4]_2[UO_2Cl_4]$, and $[PPh_4]_2[U(N^tBu)_2Cl_4]$, and an additional U 5f transition involving the $1a_{2u}$ orbital was also observed for $[PPh_4]_2[U(N^tBu)_2Cl_4]$. The DFT and XAS results agree that the total amount of Cl 3p character (%) observed with the U 5f orbitals was roughly 7−10% per U−Cl bond for both compounds, which shows that moving from oxo to imido has little effect on the amount of mixing in the U−Cl antibonding orbitals of 5f parentage. However, significantly more U−Cl mixing was calculated previously in closely related molecular systems of hexavalent uranium with fewer oxo and imido ligands, such as $[UOCl_5]^-$ (23.3% Cl 3p character for Cl in the equatorial plane)[70] and UCl_6 (30.6% Cl 3p character for four Cl atoms).[70] This reduction in 5f mixing in the equatorial plane may be a consequence of having two highly covalent U−O and U−N bonds, which cooperate to enhance 5f mixing in the axial positions through the inverse *trans*-influence.[6,15,96−99] Experiments to validate this interpretation by probing both 6d and 5f orbital mixing in the U−O and U−N^{t}Bu interactions directly using a combination of O and N K-edge XAS spectroscopy are currently underway.

ASSOCIATED CONTENT

Supporting Information

Complete ref 80, complete Cl K-edge XAS data and curve-fitting models for $[UO_2Cl_4]^{2-}$ and $[U(N^tBu)_2Cl_4]^{2-}$, CIF files for all of the reported structures, and representative unoccupied Khon−Sham orbitals (primarily 5f and 6d) for $U(NMe)_2Cl_4^{2-}$ and $UO_2Cl_4^{2-}$. This material is available free of charge via the Internet at http://pubs.acs.org.

AUTHOR INFORMATION

Corresponding Author

stosh@lanl.gov; boncella@lanl.gov; erb@lanl.gov

Notes

The authors declare no competing financial interest.

ACKNOWLEDGMENTS

This work was supported by U.S. Department of Energy, Office of Basic Energy Sciences, Division of Chemical Sciences, Geosciences, and Biosciences (Heavy Element Chemistry Program), the US Department of Energy, Office of Science Undergraduate Internship Program (SULI; MacInnes), and the Glenn T. Seaborg Institute Postdoctoral Fellowship Program (Spencer, Minasian, Jilek, Gdula, Hayton, Olson, Yang). Support was also provided by the Director, Office of Science, Office of Basic Energy Sciences, Division of Chemical Sciences, Geosciences, and Biosciences of the U.S. Department of Energy at Lawrence Berkeley National Laboratory under contract DE-AC02-05CH11231. We thank Robin L. Gdula for providing synthetic assistance. Portions of this research were carried out

at the Stanford Synchrotron Radiation Lightsource, a Directorate of SLAC National Accelerator Laboratory and an Office of Science User Facility operated for the U.S. Department of Energy Office of Science by Stanford University. The SSRL Structural Molecular Biology Program is supported by the DOE Office of Biological and Environmental Research, and by the National Institutes of Health, National Institute of General Medical Sciences (including P41GM103393) and the National Center for Research Resources (P41RR001209). Los Alamos National Laboratory is operated by Los Alamos National Security, LLC, for the National Nuclear Security Administration of U.S. Department of Energy under Contract DEAC52-06NA25396.

REFERENCES

(1) Grenthe, I.; Drodzynski, J.; Fujino, T.; Buck, E. C.; Albrecht-Schmitt, T. E.; Wolf, S. F. *Uranium In The Chemistry of the Actinide and Transactinide Elements*, 3rd ed.; Morss, L. R., Edelstein, N. M., Fuger, J., Eds.; Springer-Verlag: Berlin, 2006; Vol *1*, p 253.
(2) Ohwada, K. *J. Inorg. Nucl. Chem.* **1978**, *40*, 1369.
(3) Flint, C. D.; Tanner, P. A. *J. Chem. Soc., Faraday Trans. 2* **1978**, *74*, 2210.
(4) Baev, A. S.; Teterin, Yu. A.; Mashirov, L. G.; Suglobov, D. N. *Radiokhim.* **1986**, *28*, 460.
(5) Tatsumi, K.; Hoffmann, R. *Inorg. Chem.* **1980**, *19*, 2656.
(6) Denning, R. G. *Struct. Bonding (Berlin)* **1992**, *79*, 215.
(7) Schreckenbach, G.; Hay, P. J.; Martin, R. L. *J. Comput. Chem.* **1999**, *20*, 70.
(8) Kaltsoyannis, N. *Inorg. Chem.* **2000**, *39*, 6009.
(9) Soga, T. *Spectrochim. Acta, A* **2001**, *57A*, 1767.
(10) Denning, R. G.; Green, J. C.; Hutchings, T. E.; Dallera, C.; Tagliaferri, A.; Giarda, K.; Brookes, N. B.; Braicovich, L. *J. Chem. Phys.* **2002**, *117*, 8008.
(11) Kaltsoyannis, N. *Chem. Soc. Rev.* **2003**, *32*, 9.
(12) Clark, A. E.; Sonnenberg, J. L.; Hay, P. J.; Martin, R. L. *J. Chem. Phys.* **2004**, *121*, 2563.
(13) Sonnenberg, J. L.; Hay, P. J.; Martin, R. L.; Bursten, B. E. *Inorg. Chem.* **2005**, *44*, 2255.
(14) Pierloot, K.; van Besien, E. *J. Chem. Phys.* **2005**, *123*, 204309.
(15) Denning, R. G. *J. Phys. Chem. A* **2007**, *111*, 4125.
(16) Réal, F.; Vallet, V.; Marian, C.; Wahlgren, U. *J. Chem. Phys.* **2007**, *127*, 214302.
(17) Liu, G.; Deifel, N. P.; Cahill, C. L.; Zhurov, V. V.; Pinkerton, A. A. *J. Phys. Chem. A* **2012**, *116*, 855.
(18) Tecmer, P.; Bast, R.; Ruud, K.; Visscher, L. *J. Phys. Chem. A* **2012**, *116*, 7397.
(19) Dau, P. D.; Su, J.; Liu, H.-T.; Huang, D.-L.; Li, J.; Wang, L.-S. *J. Chem. Phys.* **2012**, *137*, 064315.
(20) Jørgensen, C. K.; Reisfeld, R. *J. Electrochem. Soc.* **1983**, *130*, 681.
(21) Jørgensen, C. K.; Reisfeld, R. *Struct. Bonding (Berlin)* **1982**, *50*, 121.
(22) Lewis, N. S.; Nocera, D. G. *Proc. Natl. Acad. Sci. U.S.A.* **2006**, *103*, 15729.
(23) Burns, C. J.; Eisen, M. S. Organoactinide Chemistry: Synthesis and Characterization. In *The Chemistry of the Actinide and Transactinide Elements*, 3rd ed.; Morss, L. R., Edelstein, N. M., Fuger, J., Eds.; Springer: Berlin, 2006; Vol. *1*, p 2799.
(24) Kaltsoyannis, N.; Hay, P. J.; Li, J.; Blaudeau, J. P.; Bursten, B. E. Theoretical studies of the electronic structure of compounds of the actinide elements. In *The Chemistry of the Actinide and Transactinide Elements*, 3rd ed.; Morss, L. R., Edelstein, N. M., Fuger, J., Katz, J. J., Eds.; Springer:Berlin, 2006; Vol. *1*, p 1893.
(25) Dao, N. Q. *Acta Crystallogr.* **1972**, *B28*, 2011.
(26) di Sipio, L.; Tondello, E.; Pelizzi, G.; Ingletto, G.; Montenero, A. *Cryst. Struct. Commun.* **1974**, *3*, 527.
(27) di Sipio, L.; Tondello, E.; Pelizzi, G.; Ingletto, G.; Montenero, A. *Cryst. Struct. Commun.* **1974**, *3*, 731. (d) di Sipio, L.; Tondello, E.; Pelizzi, G.; Ingletto, G.; Montenero, A. *Cryst. Struct. Commun.* **1974**, *3*, 297.
(28) Brown, D. R.; Chippindale, A. M.; Denning, R. G. *Acta Crystallogr.* **1996**, *C52*, 1164.
(29) Mikhailov, Y. N.; Lobanova, G. N.; Kanishcheva, A. S.; Bolotova, G. T.; Tsapkin, V. V.; Nuikin, A. Y.; Shchelokov, R. N. *Russ. J. Inorg. Chem.* **1983**, *28*, 2056.
(30) Danis, J. A.; Lin, M. R.; Scott, B. L.; Eichhorn, B. W.; Runde, W. H. *Inorg. Chem.* **2001**, *40*, 3389.
(31) di Sipio, L.; Tondello, E.; Pelizzi, G.; Ingletto, G.; Montenero, A. *Cryst. Struct. Commun.* **1974**, *3*, 297.
(32) Jensen, W.; Dickerson, D.; Johnson, Q. *Acta Crystallogr.* **1974**, *B30*, 840.
(33) Marzatto, A.; Graziani, R.; Bombieri, G.; Forsellini, E. *J. Cryst. Mol. Struct.* **1974**, *4*, 253.
(34) Bohrer, R.; Conradi, E.; Muller, U. *Z. Anorg. Allg. Chem.* **1988**, *558*, 119.
(35) Clemente, D. A.; Marzatto, A. *Acta Crystallogr.* **2003**, *B59*, 43.
(36) Conradi, E.; Bohrer, R.; Muller, U. *Chem. Ber.* **1986**, *119*, 2582.
(37) Crawford, M.-J.; Mayer, P. *Inorg. Chem.* **2005**, *44*, 5547.
(38) Denning, R. G.; Morrison, I. D. *Chem. Phys. Lett.* **1991**, *180*, 101.
(39) Denning, R. G.; Norris, J. O. W.; Brown, D. *Mol. Phys.* **1982**, *46*, 325.
(40) Denning, R. G.; Norris, J. O. W.; Brown, D. *Mol. Phys.* **1982**, *46*, 287.
(41) Gatto, C. C.; Lang, E. S.; Jagst, A.; Abram, U. *Inorg. Chim. Acta* **2004**, *357*, 4405.
(42) Gatto, C. C.; Lang, E. S.; Kupfer, A.; Hagenbachb, A.; Abram, U. *Z. Anorg. Allg. Chem.* **2004**, *630*, 1286.
(43) Abram, U.; Lang, E. S.; Bonfada, E. *Z. Anorg. Allg. Chem.* **2002**, *628*, 1873.
(44) Leverd, P. C.; Rinaldo, D.; Nierlich, M. *Dalton Trans.* **2002**, 829.
(45) Duval, P. B.; Burns, C. J.; Buschmann, W. E.; Clark, D. L.; Morris, D. E.; Scott, B. L. *Inorg. Chem.* **2001**, *40*, 5491.
(46) Burns, C. J.; Smith, W. H.; Huffman, J. C.; Sattelberger, A. P. *J. Am. Chem. Soc.* **1990**, *112*, 3237.
(47) Arney, D. S. J.; Burns, C. J.; Smith, D. C. *J. Am. Chem. Soc.* **1992**, *114*, 10068.
(48) Arney, D. S. J.; Burns, C. J. *J. Am. Chem. Soc.* **1993**, *115*, 9840.
(49) Brown, D. R.; Denning, R. G.; Jones, R. H. *Chem. Commun.* **1994**, 2601.
(50) Wagner, B. P.; Scott, B. L.; Burns, C. J. *Angew. Chem., Int. Ed.* **1998**, *37*, 959.
(51) Hayton, T. W.; Boncella, J. M.; Scott, B. L.; Palmer, P. D.; Batista, E. R.; Hay, P. J. *Science* **2005**, *310*, 1941.
(52) Hayton, T. W.; Boncella, J. M.; Scott, B. L.; Batista, E. R. *J. Am. Chem. Soc.* **2006**, *128*, 12622.
(53) Hayton, T. W.; Boncella, J. M.; Scott, B. L.; Batista, E. R.; Hay, P. J. *J. Am. Chem. Soc.* **2006**, *128*, 10549.
(54) Spencer, L. P.; Yang, P.; Scott, B. L.; Batista, E. R.; Boncella, J. M. *J. Am. Chem. Soc.* **2008**, *130*, 2930.
(55) (a) Spencer, L. P.; Gdula, R. L.; Hayton, T. W.; Scott, B. L.; Boncella, J. M. *Chem. Commun.* **2008**, 4986. (b) Jilek, R. E.; Spencer, L. P.; Lewis, R. A.; Scott, B. L.; Hayton, T. W.; Boncella, J. M. *J. Am. Chem. Soc.* **2012**, *134*, 9876.
(56) Spencer, L. P.; Schelter, E. J.; Yang, P.; Gdula, R. L.; Scott, B. L.; Thompson, J. D.; Kiplinger, J. L.; Batista, E. R.; Boncella, J. M. *Angew. Chem., Int. Ed.* **2009**, *48*, 3739.
(57) Evans, W. J.; Tralna, C. A.; Ziller, J. W. *J. Am. Chem. Soc.* **2009**, *131*, 17473.
(58) Cantat, T.; Graves, C. R.; Scott, B. L.; Kiplinger, J. L. *Angew. Chem., Int. Ed.* **2009**, *48*, 3681.
(59) Spencer, L. P.; Yang, P.; Scott, B. L.; Batista, E. R.; Boncella, J. M. *Inorg. Chem.* **2009**, *48*, 2693.
(60) Spencer, L. P.; Yang, P.; Scott, B. L.; Batista, E. R.; Boncella, J. M. *Inorg. Chem.* **2009**, *48*, 11615.
(61) Barros, N.; Maynau, D.; Maron, L.; Eisenstein, O.; Zi, G.; Andersen, R. A. *Organometallics* **2007**, *26*, 5059.

(62) Seaman, L. A.; Wu, G.; Edelstein, N.; Lukens, W. W.; Magnani, N.; Hayton, T. W. *J. Am. Chem. Soc.* **2012**, *134*, 4931.
(63) Solomon, E. I.; Hedman, B.; Hodgson, K. O.; Dey, A.; Szilagyi, R. K. *Coord. Chem. Rev.* **2005**, *249*, 97.
(64) Hedman, B.; Hodgson, K. O.; Solomon, E. I. *J. Am. Chem. Soc.* **1990**, *112*, 1643.
(65) Shadle, S. E.; Hedman, B.; Hodgson, K. O.; Solomon, E. I. *Inorg. Chem.* **1994**, *33*, 4235.
(66) Shadle, S. E.; Hedman, B.; Hodgson, K. O.; Solomon, E. I. *J. Am. Chem. Soc.* **1995**, *117*, 2259.
(67) Glaser, T.; Hedman, B.; Hodgson, K. O.; Solomon, E. I. *Acc. Chem. Res.* **2000**, *33*, 859.
(68) Kozimor, S. A.; Yang, P.; Batista, E. R.; Boland, K. S.; Burns, C. J.; Clark, D. L.; Conradson, S. D.; Martin, R. L.; Wilkerson, M. P.; Wolfsberg, L. E. *J. Am. Chem. Soc.* **2009**, *131*, 12125.
(69) Kozimor, S. A.; Yang, P.; Batista, E. R.; Boland, K. S.; Burns, C. J.; Christensen, C. N.; Clark, D. L.; Conradson, S. D.; Hay, P. J.; Lezama, J. S.; Martin, R. L.; Schwarz, D. E.; Wilkerson, M. P.; Wolfsberg, L. E. *Inorg. Chem.* **2008**, *47*, 5365.
(70) Minasian, S. G.; Keith, J. M.; Batista, E. R.; Boland, K. S.; Christensen, C. N.; Clark, D. L.; Conradson, S. D.; Kozimor, S. A.; Martin, R. L.; Schwarz, D. E.; Shuh, D. K.; Wagner, G. L.; Wilkerson, M. P.; Wolfsberg, L. E.; Yang, P. *J. Am. Chem. Soc.* **2012**, *134*, 5586.
(71) Brown, D. R.; Chippindale, A. M.; Denning, R. G. *Acta Crystallogr., Sect. C* **1996**, *52*, 1164.
(72) (a) Wilkerson, M. P.; Burns, C. J.; Paine, R. T.; Scott, B. L. *Inorg. Chem.* **1999**, *38*, 4156. (b) Wilkerson, M. P.; Burns, C. J.; Paine, R. T.; Blosch, L. L.; Andersen, R. A. *Inorg. Synth.* **2004**, *34*, 93.
(73) Shadle, S. E. Ph.D. Thesis, Stanford University, 1994.
(74) Helmholz, L.; Kruh, R. F. *J. Am. Chem. Soc.* **1952**, *74*, 1176.
(75) George, G. N. *EDG_FIT*; Stanford Synchrotron Radiation Laboratory, Stanford Linear Accelerator Center, Stanford University: Stanford, CA.
(76) Bradley, J. A.; Yang, P.; Batista, E. R.; Boland, K. S.; Burns, C. J.; Clark, D. L.; Conradson, S. D.; Kozimor, S. A.; Martin, R. L.; Seidler, G. T.; Scott, B. L.; Shuh, D. K.; Tyliszczak, T.; Wilkerson, M. P.; Wolfsberg, L. E. *J. Am. Chem. Soc.* **2010**, *132*, 13914.
(77) Daly, S. R.; Keith, J. M.; Batista, E. R.; Boland, K. S.; Clark, D. L.; Kozimor, S. A.; Martin, R. L. *J. Am. Chem. Soc.* **2012**, *134*, 14408.
(78) Becke, A. D. *J. Chem. Phys.* **1993**, *98*, 5648.
(79) Lee, C. T.; Yang, W. T.; Parr, R. G. *Phys. Rev. B.* **1988**, *37*, 785.
(80) Frisch, M. J.; et al. *Gaussian 09*, Revision B.01; Gaussian, Inc.: Wallingford, CT, 2009.
(81) Fuentealba, P.; Preuss, H.; Stoll, H.; Vonszentpaly, L. *Chem. Phys. Lett.* **1982**, *89*, 418.
(82) Kuchle, W.; Dolg, M.; Stoll, H.; Preuss, H. *Mol. Phys.* **1991**, *74*, 1245.
(83) Kuchle, W.; Dolg, M.; Stoll, H.; Preuss, H. *J. Chem. Phys.* **1994**, *100*, 7535.
(84) Ehlers, A. W.; Bohme, M.; Dapprich, S.; Gobbi, A.; Hollwarth, A.; Jonas, V.; Kohler, K. F.; Stegmann, R.; Veldkamp, A.; Frenking, G. *Chem. Phys. Lett.* **1993**, *208*, 111.
(85) Niu, S. Q.; Hall, M. B. *Chem. Rev.* **2000**, *100*, 353.
(86) Baker, J.; Muir, M.; Andzelm, J.; Scheiner, A. In *ACS Symposium Series 629*; Laird, B. B., Ross, R. B., Ziefler, T., Eds.; American Chemical Society: Washington, DC, 1996.
(87) *APEX II*, v. 1.08; Bruker AXS, Inc.: Madison, WI, 2004.
(88) *SAINT*, v. 7.06; Bruker AXS, Inc.: Madison, WI, 2003.
(89) Sheldrick, G. M. *SADABS*, v. 2.03; University of Göttingen: Göttingen, Germany, 2001.
(90) *SHELXTL*, v. 5.10; Bruker AXS, Inc.: Madison, WI, 1997.
(91) Ballhausen, C. J.; Gray, H. B. *Molecular Orbital Theory*; W. A. Benjamin, Inc.: New York, 1965.
(92) The higher lying a_{1g}, b_{1g}, and e_g orbitals of 6d parentage are heavily mixed and form bonding interactions with Cl 3p orbitals as well as N−C sp hybrids.
(93) Segala, M.; Chong, D. P. *J. Electron Spectrosc. Relat. Phenom.* **2010**, *182*, 141.
(94) Martin, R. L.; Shirley, D. A. *Electron Spectroscopy, Theory, Techniques and Applications*; Academic Press: New York, 1977; Vol. *1*, p 75.
(95) Grady, E. O.; Kaltsoyannis, N. *J. Chem. Soc., Dalton Trans.* **2002**, 1233.
(96) Minasian, S. G.; Krinsky, J. L.; Arnold, J. *Chem.—Eur. J.* **2011**, *17*, 12234.
(97) Kosog, B.; La Pierre, H. S.; Heinemann, F. W.; Liddle, S. T.; Meyer, K. *J. Am. Chem. Soc.* **2012**, *134*, 5284.
(98) Spencer, L. P; Yang, P.; Scott, B. L.; Batista, E. R.; Boncella, J. M. *C. R. Chim.* **2010**, *13*, 758.
(99) La Pierre, H. S.; Meyer, K. *Inorg. Chem.* **2012**, published online December 12, DOI: 10.1021/ic302412j.